

Computational Modeling of Induction Hardening Process of Machine Parts

Yutaka Toi and Masakazu Takagaki

Abstract— The coupled computational procedure of the induction heating, the thermal conduction, the thermal elasto-viscoplastic damage and the phase transformation analysis has been developed for the induction hardening analysis of steel machine parts. The validity of the proposed computational procedure has been illustrated by conducting the induction hardening analysis of a circular bar and a rectangular bar.

Key Words— Computational Mechanics, Finite Element Analysis, Induction Heating, Thermal Conduction, Thermal Elasto-Viscoplasticity, Phase Transformation

I. INTRODUCTION

The induction hardening is one of the methods for heat treatment of steel machine parts, which can harden only the surface of the parts and has been applied to various machine parts such as automobile components and toothed gears. In the induction hardening, the surface of the machine part is heated up to the hardening temperature by the induction heating and transformed to the austenite phase. The heated machine part is then cooled down and the surface is transformed to the martensite phase and hardened. The heating condition for the induction hardening can be determined experimentally or empirically for the machine parts of a simple shape such as circular bars. However, it is difficult to determine the optimal heating condition for the machine parts of a complex shape. Therefore the computational determination of the optimal heating condition is required.

The commercial code SYSWELD and the researches by Miyachika et al. [1] have dealt with the analysis method considering the induction heating, the thermal stresses and the phase transformation. However, there are no analytical methods which take account of the damage and conduct the three-dimensional calculations for all physical fields, considering the interactions of the fields.

The computational method considering the coupling of the induction heating, the thermal conduction, the thermal elasto-viscoplasticity and the phase transformation is formulated in the present study. The hexahedral isoparametric element is used in the three-dimensional finite

element analysis. The validity of the present computational procedure is illustrated by analyzing the induction hardening process of the machine parts of a simple shape.

II. COUPLED COMPUTATIONAL PROCEDURE

A. Induction Heating

In the induction hardening, the objects are heated by the eddy current which is generated by the electro-magnetic induction. The distribution of the eddy current density is calculated by the electro-magnetic analysis. The method of magnetic vector potential (the $\mathbf{A} - \phi$ method) is employed in the present analysis [2]. The governing equations for the $\mathbf{A} - \phi$ method, which are expressed in terms of the magnetic vector potential \mathbf{A} and the electric scalar potential ϕ , are given by the following equations:

$$\nabla \times \left(\frac{1}{\mu} \nabla \times \mathbf{A} \right) = \mathbf{J}_0 - \sigma_c \left(\frac{\partial \mathbf{A}}{\partial t} + \nabla \phi \right) \quad (1)$$

$$\nabla \cdot \sigma_c \left(\frac{\partial \mathbf{A}}{\partial t} + \nabla \phi \right) = 0 \quad (2)$$

where \mathbf{J}_0 , μ and σ_c are the forced current, the magnetic permeability and the permittivity respectively [3]. The terms including the partial time derivative $\partial/\partial t$ can be replaced with the complex variable expression $j\omega$ when treating the alternating current problems. The uniqueness of solutions for eq. (1) can be guaranteed by substituting Coulomb gauge $\nabla \cdot \mathbf{A} = 0$. The consideration of these in Equations (1) and (2) leads to the following equations:

$$\frac{1}{\mu} \nabla^2 \mathbf{A} = -\mathbf{J}_0 + \sigma_c (j\omega \mathbf{A} + \nabla \phi) \quad (3)$$

$$\nabla \cdot \sigma_c (j\omega \mathbf{A} + \nabla \phi) = 0 \quad (4)$$

The eddy current density is calculated by discretizing Equations (3) and (4) with the Galerkin finite element method [1]. The eddy current density \mathbf{J}_e is expressed in terms of the magnetic vector potential \mathbf{A} and the electric scalar potential ϕ given by the electromagnetic analysis as shown in the following equation:

$$\mathbf{J}_e = \sigma_c (j\omega \mathbf{A} + \nabla \phi) \quad (5)$$

By using the obtained eddy current density, the thermal release Q_e is defined as follows:

Manuscript received July 2, 2008.

Y. Toi is with the Institute of Industrial Science, University of Tokyo, Komaba, Meguro-ku, Tokyo, 153-8505 Japan (phone: 03-5452-6178, fax: 03-5452-6180, e-mail: toi@iis.u-tokyo.ac.jp).

M. Takagaki is with the Institute of Industrial Science, University of Tokyo, Komaba, Meguro-ku, Tokyo, 153-8505 Japan.

$$Q_e = \int_V \frac{1}{\sigma_c} |\mathbf{J}_e|^2 dV \quad (6)$$

which gives the boundary condition for the thermal conduction analysis in the heating process.

B. Thermal Conduction

In the thermal conduction analysis, the Galerkin finite element method is applied to the governing equations with the central difference time marching scheme. The thermal conductivity of a solid is influenced by the microscopic damage such as microvoids and microcracks. The thermal conductivity λ^{eq} considering the effect of damage [4] as given by the following equation is employed in the present analysis:

$$\lambda^{eq} = \lambda_0(1-D) + d\tilde{\lambda}^{rad} \quad (7)$$

where λ_0 and D are the thermal conductivity of an undamaged solid and the damage variable, respectively. The term $d\tilde{\lambda}^{rad}$ indicates the effect of thermal radiation as given by the following equation:

$$d\tilde{\lambda}^{rad} = \sigma_B \varepsilon_0 \left(4DT^3 + \frac{\partial D / \partial \mathbf{x}}{\partial T / \partial \mathbf{x}} T^4 \right) d\mathbf{x} \quad (8)$$

where σ_B , ε_0 and T are Boltzman constant, the emissivity and the temperature respectively. The thermal conductivity of eq. (7) is introduced in the thermal conduction equation, in which λ_0 and the density ρ are assumed as follows considering the effect of phase transformation:

$$\lambda_0 = \sum_{I=1}^3 \xi_I \lambda_I \quad (9)$$

$$\rho = \sum_{I=1}^3 \xi_I \rho_I \quad (10)$$

where ξ_I , λ_I and ρ_I are respectively the volume fraction, the thermal conductivity and the density for each phase ($I = 1$; austenite, $I = 2$; pearlite, $I = 3$; martensite).

C. Thermal Elasto-Viscoplasticity

The constitutive equations based on continuum damage mechanics and the creep-plasticity isotropic hardening theory are extended to take account of the effect of phase transformation and the temperature dependence in the present study.

The elastic constitutive equation is given as follows [5]:

$$\boldsymbol{\varepsilon} = \frac{1+\nu}{E} \frac{\boldsymbol{\sigma}}{1-D} - \frac{\nu}{E} \left(tr \frac{\boldsymbol{\sigma}}{1-D} \right) \mathbf{1} + \alpha \Delta T \mathbf{1} + \sum_{I=1}^L \xi_I \beta_I \mathbf{1} \quad (11)$$

where

$$\alpha = \sum_{I=1}^3 \xi_I \alpha_I \quad (12)$$

In eq. (11), $\boldsymbol{\varepsilon}$, $\boldsymbol{\sigma}$ and $\mathbf{1}$ are respectively the strain tensor, the stress tensor and the unit tensor. E , ν , ΔT and β_I are Young's modulus, Poisson's ratio, the temperature increment and the volume expansion rate due to the phase transformation for each phase, respectively. The thermal expansion coefficient α is given by eq. (12), using the

volume fractions and the thermal expansion coefficients for each phase.

The viscoplastic strain is given by the following equations, based on the creep-plasticity isotropic hardening theory [6-9],

$$\boldsymbol{\varepsilon}_{vp} = \frac{3}{2} \left\langle \frac{\sigma_{eq} / (1-D) - R - k}{K} \right\rangle^N \frac{\boldsymbol{\sigma}'}{\sigma_{eq}} \quad (13)$$

where

$$R = Q_1 p + Q_2 [1 - \exp(-bp)] \quad (14)$$

In eqs. (13) and (14), the following notations are used: $\boldsymbol{\varepsilon}_{vp}$; the viscoplastic strain tensor, σ_{eq} ; von Mises equivalent stress, R ; the isotropic hardening parameter, k ; the initial yield stress, $\boldsymbol{\sigma}'$; the deviatoric stress tensor, p ; the accumulated equivalent plastic strain, K , N , Q_1 , Q_2 and b ; the material constants. The initial yield stress k considering the effect of the phase transformation is given by the following equation:

$$k = \sum_{I=1}^3 \xi_I k_I \quad (15)$$

where k_I is the initial yield stress for each phase.

The scalar damage evolution equation is given by the following equations [5]:

$$\dot{D} = \left(-\frac{Y}{S} \right)^s \dot{p} \quad (16)$$

where

$$-Y = \frac{1}{2E(1-D)^2} \left[\frac{2}{3}(1+\nu)\sigma_{eq}^2 + 3(1-2\nu)\sigma_H^2 \right] \quad (17)$$

in which Y and σ_H are the strain energy density release rate and the hydrostatic pressure, respectively. S and s are the material constants.

D. Phase Transformation

The austenite, pearlite and martensite phase are considered as the microstructure of steels in the present study. The volume fractions for the austenite, pearlite and martensite phase are denoted by ξ_1 , ξ_2 and ξ_3 , respectively. Their evolution equations are discussed below.

The martensite transformation and the pearlite transformation mainly take place in the process of induction hardening. Based on Magee [10], the evolution equation for the martensite phase is given as follows [11]:

$$\xi_3 = (1 - \xi_2)(1 - A_r) [1 - \exp\{\phi(T)\}] \quad (18)$$

where the temperature-dependent function $\phi(T)$ is given by the following equation for S45C steel:

$$\phi(T) = \begin{cases} -0.544 \times 10^{-4} (M_s - T)^2 & \text{for } (M_s - T) \leq 77 \\ -0.231 \times 10^{-1} (317 - T) & \text{for } (M_s - T) > 77 \end{cases} \quad (19)$$

In eq. (19), M_s ($=380^\circ\text{C}$) is the critical starting temperature of martensite transformation. ξ_2 is the volume fraction of the pearlite phase which was generated before the starting of the martensite transformation. A_r is the volume fraction of

the residual austenite phase which is only subjected to the martensite transformation.

The evolution equation for the pearlite transformation is formulated by the following equation, based on the concept of Johnson-Mehl:

$$\xi_2 = 1 - \exp(-V_e) \quad (20)$$

where V_e is expressed as follows, using the temperature-dependent function $f(T)$:

$$V_e = \int_0^t \frac{4}{3} \pi G^3 (t - t_1) \dot{N} dt_1 = \int_0^t f(T) (t - t_1)^3 dt_1 \quad (21)$$

In eq; (10), G and \dot{N} are the nuclear growth rate and the nuclear generation rate respectively. The function $f(T)$ is experimentally determined for S45C as follows:

$$f(T) = -0.071 \left(\frac{T - 380}{145} \right)^{6.91} \left(\frac{720 - T}{195} \right)^{9.31} \quad (22)$$

The volume fraction of the austenite phase is calculated as $\xi_1 = 1 - (\xi_2 + \xi_3)$ (23)

Figure 1 shows the coupled computational procedure for the induction heating, the thermal conduction, the elasto-viscoplastic damage and the phase transformation analysis. The electromagnetic analysis, the thermal conduction analysis and the elasto-viscoplastic damage analysis are sequentially conducted in the heating process of the induction hardening, while the phase transformation analysis, the thermal conduction analysis and the elasto-viscoplastic damage analysis are sequentially carried out in the cooling process. The above-mentioned sequential (or weakly coupled) approach is repeated with a small time increment from the initial to the final stage.

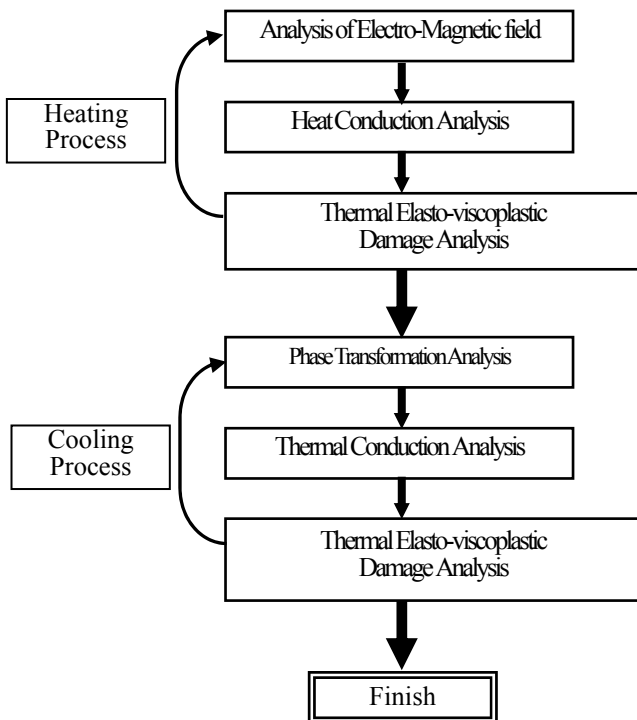


Fig. 1 Sequential approach for coupled analysis

III. ANALYSIS OF INDUCTION HARDENING

A. Induction Hardening of a Circular Bar

Figure 2 shows the analyzed circular steel bar with a radius of 10mm and a length of 20mm. The heating coil is made of copper. Considering the symmetry, the part of 1/2 in the axial direction and 1/72 in the circumferential direction is subdivided into eight node, hexahedral isoparametric elements as shown in Fig. 3. The surrounding air region of three times larger than the circular bar and the heating coil in the axial and the radial direction is assumed for the electromagnetic analysis. The numbers of elements and nodes are 1188 and 1938 respectively.

The circular bar is heated from the room temperature (20°C) to the hardening temperature (930°C) and cooled down in the water of 20°C. The frequency and the electric power for the induction coil are 200kHz and 50kW respectively. Table 1 shows the material constants for the analysis including the thermal conductivity, the density and the thermal expansion coefficient for each phase.

Figure 4 shows the distribution of eddy current density in the circular bar calculated by the electromagnetic analysis. It is seen from the figure that the large eddy current flows in the neighborhood of the surface of the bar. Figure 5 shows the calculated time-histories of temperature (d : the radial distance from the surface), which are compared with the numerical results given by Miyachika et al. [1] to illustrate the validity of the present computational procedure. Figure 6 shows the time-histories of the axial stress, from which it is seen that the large compressive stress takes place near the bar surface at the induction heating process and turns into the tensile stress at the cooling process, resulting in the large residual stress at the finishing of the hardening process.

Figure 7 shows the contour of von Mises equivalent stress on the radial cross-section when the temperature becomes almost constant after cooling, from which it is seen that the large residual stress occurs near the bar surface. Figure 8 shows the distribution of the volume fraction of martensite phase (the hardening layer) at the same stage as Fig. 7. The result in Fig. 8 can be considered to be qualitatively reasonable.

Table 1. Material constants

	Austenite	Pearlite	Martensite
Heat Conductivity (W/mm°C)	29.1	35.2	39.9
Density (kg/m ³)	8150.0	7850.0	7800.0
Coefficient of thermal expansion (1/°C)	2.083×10 ⁻⁵	1.521×10 ⁻⁵	0.688×10 ⁻⁵
Young's Modulus (GPa)	206.0		
Poisson's Ratio	0.3		
Heat Transfer Rate (W/(m ² ·K))	5814.0		
Thermal Emissivity	0.79		

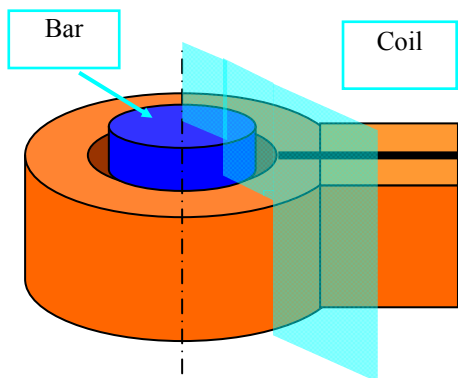


Fig. 2 Circular bar under induction hardening

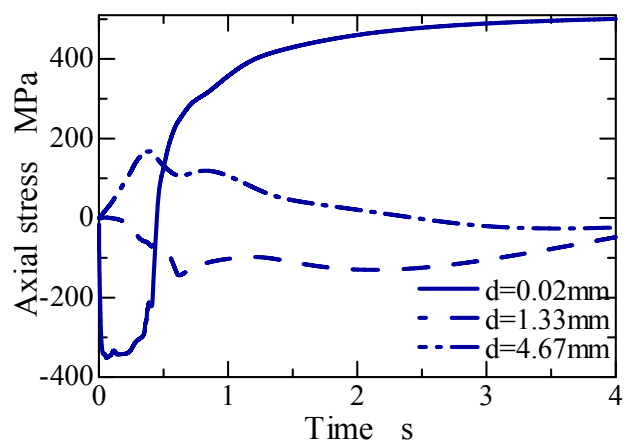


Fig. 6 Time history of axial stress

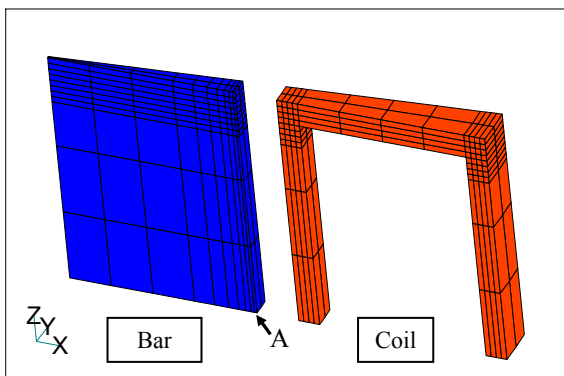


Fig. 3 Mesh subdivision

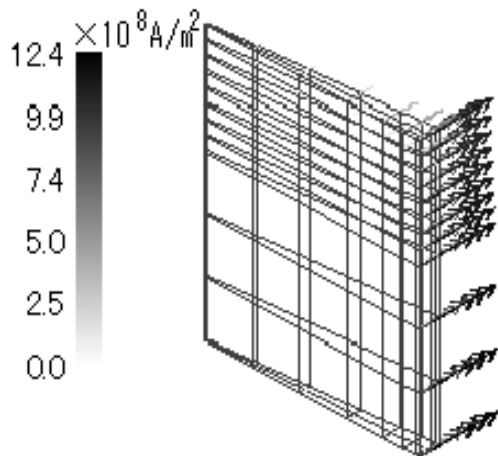


Fig. 4 Distribution of eddy current density

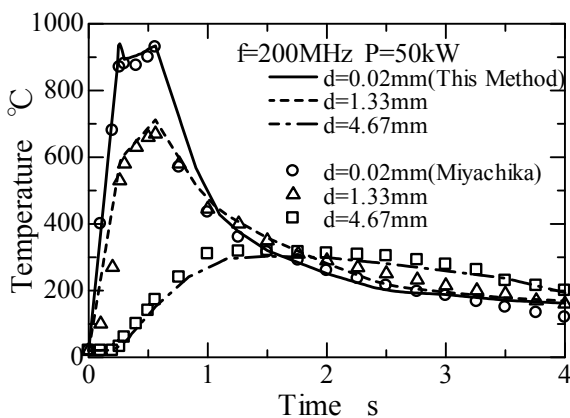


Fig. 5 Time histories of temperature

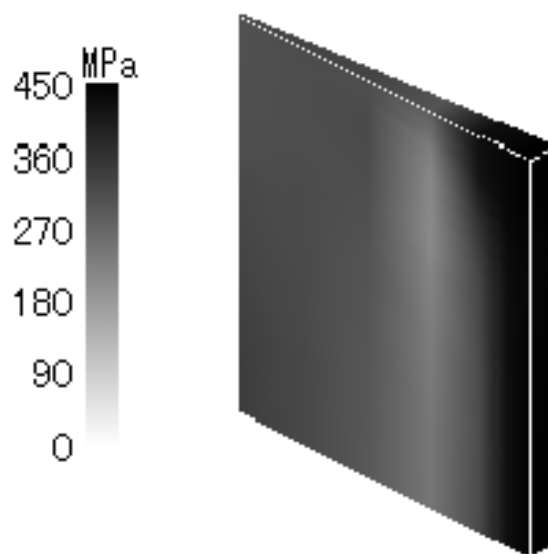


Fig. 7 Equivalent stress contour

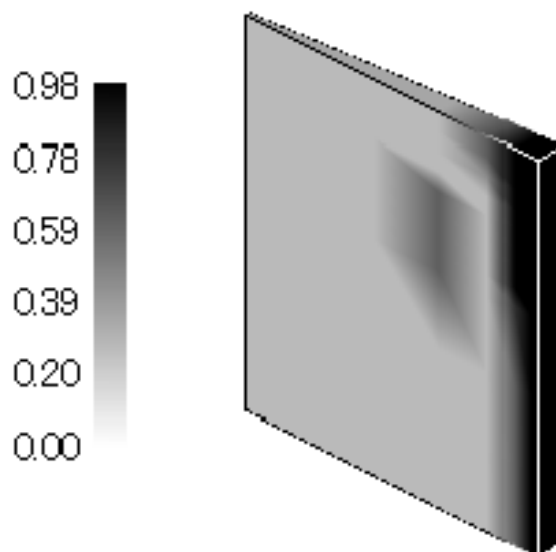


Fig. 8 Distribution of martensite phase

B. Induction Hardening of a Rectangular Bar

The third example is the induction hardening analysis of rectangular bar. Figure 9 shows the analyzed 1/4 model for the rectangular bar and the heating coil. The numbers of elements and nodes are 1740 and 2184 respectively. The analytical condition and the material constants are the same as those in the preceding subsections. Figure 10 shows the distribution of the eddy current density. The eddy current at the corners is relatively small probably because the rectangular bar is heated by the circular coil. Figures 11 and 12 show the temperature distribution at the cooling process and the distribution of the martensite volume fraction respectively, from which it is seen that the martensite volume fraction is high in the region near the surface where the temperature is lower than the starting temperature for the martensite transformation.

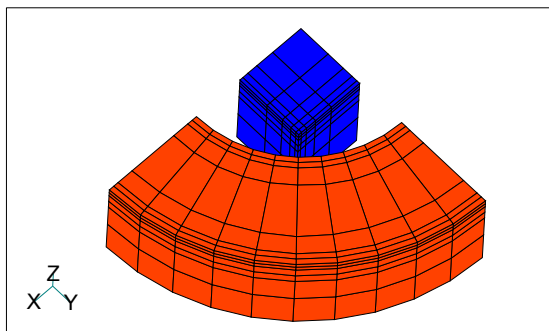


Fig. 9 Mesh Model

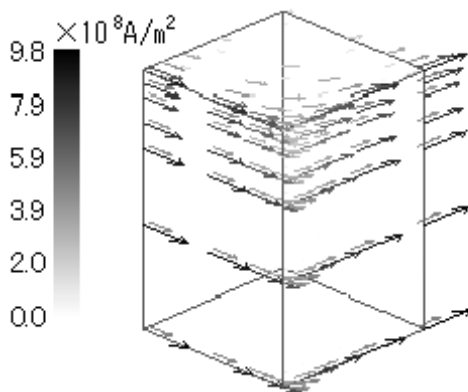


Fig. 10 Distribution of Eddy Current Density

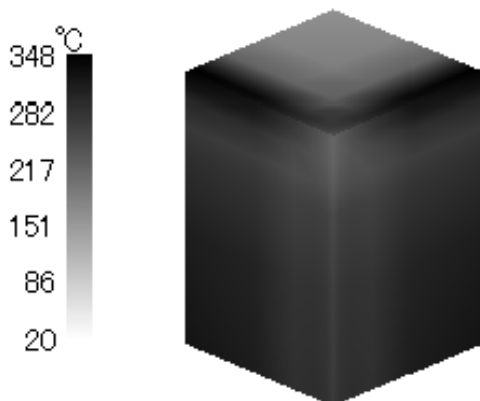


Fig. 11 Distribution of Temperature

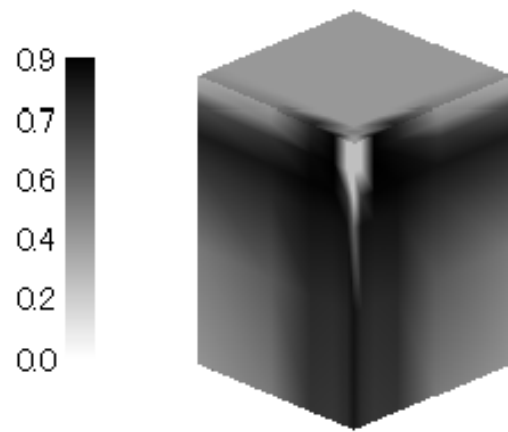


Fig. 12 Distribution of Martensite Phase

IV. CONCLUSION

The coupled computational procedure of the induction heating, the thermal conduction, the thermal elasto-viscoplastic and the phase transformation analysis has been developed for the induction hardening analysis of machine parts. The validity of the present computational procedure has been illustrated by conducting the induction hardening analysis of a circular bar and a rectangular bar. The developed computational program is also applicable to the thermal cracking analysis as well as the induction hardening analysis, as it considers the damage evolution, based on the concept of damage mechanics.

REFERENCES

- [1] Y. Miyachika et al., "Temperature and Stress During Induction Hardening Process of Smooth Axis", *Transaction of the JSME (A)*, **64**(625), 1998, pp.3623-3629.
- [2] H. Tsuboi and T. Naito, *Practical Method for Electro-Magnetic Analysis*, Yokendo, 1995.
- [3] S. Chikazumi, *Physics of Ferromagnetic Solid (Volume 1)*. Shokabo, 1991
- [4] J. Skrzypek and A. Ganczarski, "Modeling of Damage Effect on Heat Transfer in Time-Dependent Non-Homogeneous Solids", *J. of Thermal Stresses*, **21**(3), 1998, pp.205-231.
- [5] J. Lemaitre and J. L. Chaboche, *Mechanics of Solid Materials*, Cambridge University Press, 1990.
- [6] J. L. Chaboche and G. Rousselier, "On the Plastic and Viscoplastic Constitutive Equations (Part 1: rules developed with internal variable concept)", *Journal of Pressure Vessel Technology*, **105**, 1983, pp.153-164.
- [7] F. P. E. Dunne and D. R. Hayhurst, "Continuum Damage Based Constitutive Equations for Copper Under High Temperature Creep and Cyclic Plasticity", *Proc. R. Soc. Lond. A*, **437**, 1992, pp.545-566.
- [8] Y. Toi and J.-M. Lee, "Three-Dimensional Damage Analysis of Structural Members in Molten-Zinc Galvanization", *Transaction of the JSME (A)*, **66**(643), 2000, pp. 618-625.
- [9] Y. Toi and J.-M. Lee, "Thermal Elasto-Viscoplastic Damage Behavior of Structural Members in Hot-Dip Galvanization", *Int. J. of Damage Mechanics*, **11**(2), 2002, pp.171-185.
- [10] C. L. Magee, *Phase Transformation*. ASM, Chaper 3, 1968, pp.115..
- [11] T. Kishino, S. Nagaki and T. Inoue, "Phase Transformation", Thermal Conduction and Elasto-Plastic Stress in Hardening of Steel, *Materials*, **28**(312), 1979, pp.861-867.
- [12] H. Hosoda, and S. Miyazaki, "Recent Topics of Shape Memory Materials and Related Technology," *Journal of the Japan Society of Mechanical Engineers*, Vol. 107, No. 1028, 2004, pp. 509-515.